UNIVERSIDAD DE CONCEPCIÓN

Centro de Investigación en Ingeniería Matemática (CI²MA)

A perfectly matched layer for finite-element calculations of diffraction by metallic surface-relief gratings

Cinthya Rivas, Rodolfo Rodríguez,
Manuel Solano

PREPRINT 2017-10

SERIE DE PRE-PUBLICACIONES

A perfectly matched layer for finite-element calculations of diffraction by metallic surface-relief gratings

Cinthya Rivas[a], Rodolfo Rodríguez[a], Manuel E. Solano[a,*]

[a] *CI²MA and Departamento de Ingeniería Matemática, Universidad de Concepción, Concepción, Chile*

Abstract

We introduce a perfectly matched layer approach for finite element calculations of diffraction by metallic surface-relief gratings. We use a non-integrable absorbing function which allows us to use thin absorbing layers which reduce the computational time when simulating this type of structure. In addition, we numerically determine the best choice of the absorbing layer parameters and show that they are independent of the wavelength.

Keywords: periodic diffraction grating, perfectly matched layer, finite element method

1. Introduction

Thin film photovoltaic (PV) devices comprising a periodically corrugated metallic backreflector have become of interest over the last three decades [1, 2, 3, 4, 5, 6, 7, 8]. The purpose of this periodic surface-relief grating is to excite surface plasmonic polariton (SPP) waves and thereby enhance the electromagnetic field in the structure. Recently, solar devices based on one dimensional surface-relief gratings have been proposed and studied numerically: amorphous silicon thin film tandem solar cell [6], rugate filters [9, 10], periodic multilayered isotropic dielectric material on top of the metallic backreflector [8], among others. Moreover, numerical optimization of optical and geometric parameters

---

has been performed in order to maximize quantities of interest such as light absorption, solar-spectrum-integrated power-flux density and spectrally averaged electron-hole pair density [11, 12]. Computing these quantities requires solving Maxwell's equations in the frequency domain for each wavelength in the spectral regime. In addition, during an optimization process, the equations must be solved for a range of parameters, which might be computationally expensive. That is why efficient numerical methods for frequency-domain Maxwell's equations must be developed. Well known numerical techniques are the exact modal method [13], the commonly used method of moments [14, 15], the rigorous coupled-wave approach (RCWA) [16, 17], the finite element method (FEM) [18], and the finite-difference time-domain (FDTD) method [19]

In this work we focus on FEM applied to one dimensional grating problems since it is suitable for simulating complicated structures such us devices comprising different materials and surface-relief shapes [11, 12]. Roughly speaking, after decoupling the two polarization states, TE (transverse electric) and TM (transverse magnetic), the problem reduces to solving two Helmholtz equations on the xz-plane. Because of the periodicity of the grating and the quasi-periodicity of the solution, the unbounded domain is truncated in the x-direction using quasi-periodic boundary conditions on the vertical walls. In the z-direction, the truncation of the domain must be done in such a way that outward propagating waves are chosen. This can be achieved, for example, through suitable approximations of the Dirichlet-to-Neumann (DtN) operators. For instance, the technique implemented in [11] and [12] considers a Fourier-FEM approach that involves a finite element approximation inside the device and a representation of the DtN operators based on a Fourier series expansion of the fields in the unbounded regions above and below the structure. Its main drawback is the potentially high computational cost since the equations need to be solved as many times as the number of terms in the truncated Fourier series. In addition this approach does not scale well to three dimension. We refer to [20, Section 3C], for further details.

In this work we propose a different approach that uses a perfectly matched

2

layer (PML) placed above and below the structure. A PML is an artificial layer that absorbs the outward propagating waves. In this case, the equations will be solved in a slightly bigger domain but only once, which might lead to a significant reduction of the computational cost. A PML approach with integrable absorption function applied to grating problems has been introduced in [21]. There, the PML attenuates both outgoing and evanescent waves thanks to a suitable choice of the complex-valued absorbing function. In addition, numerical results reported in [21] are robust with respect to the thickness of the PML and a thickness between 50% and 150% of the grating period produces satisfactory results. On the other hand, in the context of time-harmonic acoustic scattering problems, a PML based on an absorbing function with unbounded integral has been introduced in [22]. This PML is also robust and able to absorb plane waves without any spurious reflection (see [23, 24] for further analysis and results). Moreover, since the integral of the absorbing function is infinite, the outgoing waves are rapidly absorbed, allowing us to use a PML with thickness significantly smaller than that of [21]. Furthermore, we show that the PML from [22] may be used to absorb both evanescent and propagating modes.

Based on the idea in [22], we propose and numerically study a PML with a non-integrable absorbing function applied to a structure comprising a periodic multilayered isotropic dielectric material on top of a metallic backreflector. The same technique can easily be applied to other structures as mentioned above ([6, 8, 9, 10, 11, 12]). The rest of this paper is organized as follows. First, the model problem is specified in Section 2. Then, the PML technique is introduced in Section 3 with the corresponding FEM discretization introduced in Section 4. In Section 5 we consider two examples to test the proposed PML and we end with some concluding remarks in Section 6.

2. Model setting

The problem of electromagnetic wave diffraction is based on solving Maxwell's equations in the three-dimensional Euclidean space occupied by a diffraction

grating:

$$\nabla \times \boldsymbol{E} = i\omega\mu_0\boldsymbol{H},$$
$$\nabla \times \boldsymbol{H} = -i\omega\varepsilon_0\varepsilon_r\boldsymbol{E}, \tag{1}$$

where $\boldsymbol{E}$ and $\boldsymbol{H}$ are the electric and magnetic fields respectively. Here, an exp$(-i\omega t)$ dependence on time t is implicit, with ω denoting the angular frequency. The free-space wavenumber, the free-space wavelength, and the intrinsic impedance of the free space are denoted by $k_0 := \omega\sqrt{\varepsilon_0\mu_0}$, $\lambda_0 := 2\pi/k_0$, and $\eta_0 := \sqrt{\mu_0/\varepsilon_0}$, respectively, with μ_0 being the permeability and ε_0 the permittivity of free space. The relative electric permittivity ε_r is a piecewise constant function specified below. In this paper vectors are in boldface, Cartesian unit vectors are identified as $\hat{\boldsymbol{u}}_x$, $\hat{\boldsymbol{u}}_y$ and $\hat{\boldsymbol{u}}_z$, and the position vector reads $\boldsymbol{r} = x\hat{\boldsymbol{u}}_x + y\hat{\boldsymbol{u}}_y + z\hat{\boldsymbol{u}}_z$.

The solar-cell structure is assumed to occupy the region $\Phi := \{\boldsymbol{r} \in \mathbb{R}^3 : 0 < z < L_t := L_d + L_g + L_m\}$ with the notation shown in Fig. 1. Within this region, the relative permittivity ε_r is a periodic function of $x \in (-\infty, \infty)$ with period L and also varies with $z \in \Phi$ but not with $y \in (-\infty, \infty)$; consequently, $\varepsilon_r(x, z) = \varepsilon_r(x \pm mL, z)$, $m \in \mathbb{Z}$. The half-spaces $\{\boldsymbol{r} \in \mathbb{R}^3 : z < 0\}$ and $\{\boldsymbol{r} \in \mathbb{R}^3 : z > L_t\}$ are occupied by air; hence, the relative permittivity $\varepsilon_r(x, z) \equiv 1$ in both half-spaces. The region $0 < z < L_d$ is occupied by a periodic multilayered isotropic dielectric (PMLID) material comprising M layers, as shown in Fig. 1. The relative permittivity is constant on each of this layers. The region $L_d + L_g < z < L_t$ is occupied by a spatially homogeneous metal with relative permittivity ε_m and thickness L_m. Finally, the region $L_d < z < L_d + L_g$ contains a periodically corrugated metal/dielectric interface of period L along the x axis. The relative permittivity in this zone is either ϵ_m or that of the first layer of the dielectric material as Fig. 1 also shows.

Since the domain is infinite in the y-direction, and the solution does not depend on this variable, we can consider a two-dimensional cross-section parallel to the xz-plane. In such a case, the Maxwell system can be simplified by considering the two fundamental polarizations:
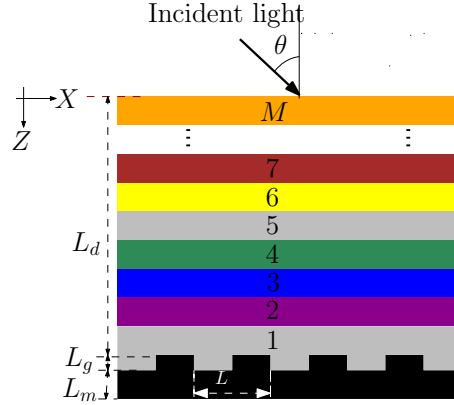
Figure 1: Schematic of of the structure considering a cross-section parallel to the xz-plane. M layers of an L_d- thick PMLID material on top of an L-periodic surface-relief grating of height L_g. A metallic backreflector of thickness L_m is below the grating. An incoming light is incident to the structure with angle θ.

- **Transverse Electric mode (TE) or s-polarization state**. The electric field $\boldsymbol{E}$ is parallel to the y axis: $\boldsymbol{E} = (0, E_y, 0)$, where E_y is independent of y, and the magnetic field is given by $\boldsymbol{H} = (H_x, 0, H_z)$; so from (1) E_y satisfies the Helmholtz problem

$$\Delta E_y + k_0^2 \varepsilon_r E_y = 0. \tag{2}$$

- **Transverse Magnetic mode (TM) or p-polarization state**. The magnetic field $\boldsymbol{H}$ is parallel to the y axis: $\boldsymbol{H} = (0, H_y, 0)$, where H_y is independent of y, and the electric field is given by $\boldsymbol{E} = (E_x, 0, E_z)$; so from (1) H_y satisfies

$$\nabla \cdot \left(\frac{1}{\varepsilon_r} \nabla \left(-\eta_0 H_y \right) \right) - k_0^2 \eta_0 H_y = 0. \tag{3}$$

The boundary $z = 0$ of the structure is illuminated by an obliquely incident plane wave whose electric field phasor is given by

$$\boldsymbol{E}_{\mathrm{inc}}(\boldsymbol{r}) = [a_s \hat{\boldsymbol{u}}_y + a_p(-\hat{\boldsymbol{u}}_x \cos\theta + \hat{\boldsymbol{u}}_z \sin\theta)] \times \exp\{ik_0[x\sin\theta + z\cos\theta]\}, \quad z \leq 0, \tag{4}$$

and the corresponding magnetic field phasor by

$$\boldsymbol{H}_{\mathrm{inc}}(\boldsymbol{r}) = \frac{1}{i\omega\mu_0}\nabla \times \boldsymbol{E}_{\mathrm{inc}}(\boldsymbol{r}), \quad z \le 0. \tag{5}$$

Here, θ is the angle of incidence with respect to the z-axis, a_s is the amplitude of the s-polarized component, and a_p the amplitude of the p-polarized component, all of them are data of the problem.

Eqs. (2) and (3) can be written in a common form as the following Helmholtz equation:

$$\nabla \cdot \left(B\nabla u\right) + k_0^2 bu = 0 \quad \text{in } \mathbb{R}^2, \tag{6}$$

where $u = E_y$, $B = 1$ and $b = \varepsilon_r$ for the s-polarization state; and $u = -\eta_0 H_y$, $B = \dfrac{1}{\varepsilon_r}$ and $b = 1$ for the p-polarization state. All of these being functions of x and z but not of y.

The periodic character of the coefficients and the quasi-periodic incident wave allow us to restrict the problem to a period $0 < x < L$, with a solution satisfying the quasi-periodicity conditions

$$\left.\begin{array}{l} u(L, z) = \exp(i\alpha L)u(0, z), \\[2mm] \dfrac{\partial u}{\partial x}(L, z) = \exp(i\alpha L)\dfrac{\partial u}{\partial x}(0, z), \end{array}\right\} \quad z \in \mathbb{R}, \tag{7}$$

where $\alpha := k_0 \sin\theta$. In addition, the strip $(0, L) \times \mathbb{R}$ is also truncated to $\Omega := (0, L) \times (0, L_t)$ and the effect of the radiation conditions at infinity must be properly taken into account. In particular, we will use a PML approach to reduce the problem to a bounded domain by truncation in z-direction. To do this we will have to consider also appropriate transmission condition on $z = 0$ and $z = L_t$.

Summarizing, we are lead to solve two problems, one for the s-polarization and the other for the p-polarization. The data of each of these two problems are computed from the corresponding components of the incident plane wave (4):

$$u_{\mathrm{inc}} = \left\{ \begin{array}{l} a_s \exp\{ik_0[x\sin\theta + z\cos\theta]\}, \text{ for the } s\text{-polarization}, \\[2mm] a_p \exp\{ik_0[x\sin\theta + z\cos\theta]\}, \text{ for the } p\text{-polarization}. \end{array} \right. \tag{8}$$

6

3. A PML approach

As stated above, the radiation conditions at infinity will be modeled by means of the perfectly matched layer technique similar to that from [22]. It is based on placing absorbing layers of anisotropic damping material above and below the domain of interest Ω, which absorb the scattered field transmitted to the exterior of the domain. We introduce two PML domains: $\Omega_-^A := (0, L) \times (-\delta_1, 0)$ and $\Omega_+^A := (0, L) \times (L_t, L_t + \delta_2)$, $\delta_1, \delta_2 > 0$ (see Fig. 2). We denote the whole PML domain by $\Omega^A := \Omega_-^A \cup \Omega_+^A$. Let Γ_- and Γ_+ denote the interfaces between the physical domain and the layers, and Γ_-^A and Γ_+^A the outer boundaries. We set u^A to be the solution in the PML domain Ω^A. Note that the PML layers directly contact the structure with no air layers.
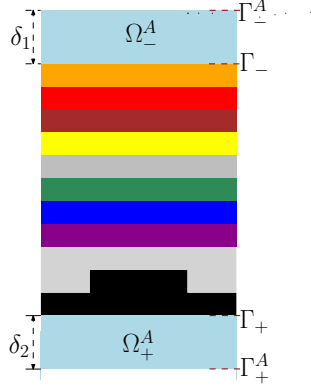

Figure 2: Domain with PML layers in Ω_+^A and Ω_-^A of thicknesses δ_1 and δ_2, resp. Γ_+ and Γ_- denote the interface between the physical domain and the PML regions. Γ_+^A and Γ_-^A correspond to the outer top and bottom boundaries.

We consider a PML method, where the unknown u^A in the absorbing layers satisfies the equation

$$\frac{\partial^2 u^A}{\partial x^2} + \frac{1}{\gamma} \frac{\partial}{\partial z} \left(\frac{1}{\gamma} \frac{\partial u^A}{\partial z} \right) + k_0^2 u^A = 0 \quad \text{in } \Omega^A,$$

where γ is an appropriate function to be specified. In order to attenuate both, outgoing and evanescent waves, it is shown in [21] that γ must be chosen as

$\gamma = \sigma_1 + i\sigma_2$, with σ_1 and σ_2 both functions of z with large integrals in both parts of the PML domain. On the other hand, it is shown in [22] that it is preferable to choose as σ_2 an unbounded function with infinite integral. We propose the following choice:

$$\gamma(z) := \begin{cases} 1, & z \in (0, L_t), \\ (1+i)\sigma(z), & z \in (-\delta_1, 0) \cup (L_t, L_t + \delta_2), \end{cases}$$

where the variable absorption coefficient $\sigma(z)$ is a non-integrable function such that

$$\int_{-\delta_1}^{0} \sigma(s)ds = +\infty \quad \text{and} \quad \int_{L_t}^{L_t+\delta_2} \sigma(s)ds = +\infty.$$

In particular, based on the numerical experimentation reported in [22], we choose the unbounded smooth positive function $\sigma : (-\delta_1, 0) \cup (L_t, L_t + \delta_2) \to \mathbb{R}$ defined by

$$\sigma(z) := \begin{cases} \dfrac{1}{\beta k_0(z + \delta_1)}, & z \in (-\delta_1, 0), \\ \dfrac{1}{\beta k_0(L_t + \delta_2 - z)}, & z \in (L_t, L_t + \delta_2), \end{cases} \tag{9}$$

where the parameter β will be determined experimentally in order to minimize the error introduced by this PML technique.

According to the results from [22] the use of this PML should lead to exact results, up to discretization errors. This agrees with more recent results from [21] where it is shown that the error in the solution obtained by using a PML is inversely proportional to the integral of σ (see Theorem 2.4 from [21]).

Altogether, u and u^A will be the solution of the following equations:

$$
\begin{cases}
\nabla \cdot (B\nabla u) + k_0^2 bu = 0 & \text{in } \Omega, \\[2mm]
\frac{\partial^2 u^A}{\partial x^2} + \frac{1}{\gamma}\frac{\partial}{\partial z}\left(\frac{1}{\gamma}\frac{\partial u^A}{\partial z}\right) + k_0^2 u^A = 0 & \text{in } \Omega^A, \\[2mm]
u(L,z) = e^{i\alpha L} u(0,z), & z \in (0, L_t), \\[2mm]
u^A(L,z) = e^{i\alpha L} u^A(0,z), & z \in (-\delta_1, 0) \cup (L_t, L_t + \delta_2), \\[2mm]
\frac{\partial u}{\partial x}(L,z) = e^{i\alpha L}\frac{\partial u}{\partial x}(0,z), & z \in (0, L_t), \\[2mm]
\frac{\partial u^A}{\partial x}(L,z) = e^{i\alpha L}\frac{\partial u^A}{\partial x}(0,z), & z \in (-\delta_1, 0) \cup (L_t, L_t + \delta_2), \\[2mm]
u = u^A + u_{\text{inc}} & \text{on } \Gamma_-, \\[2mm]
u = u^A & \text{on } \Gamma_+, \\[2mm]
B\frac{\partial u}{\partial z} = \frac{1}{\gamma}\frac{\partial u^A}{\partial z} + \frac{\partial u_{\text{inc}}}{\partial z} & \text{on } \Gamma_-, \\[2mm]
B\frac{\partial u}{\partial z} = \frac{1}{\gamma}\frac{\partial u^A}{\partial z} & \text{on } \Gamma_+, \\[2mm]
u^A = 0 & \text{on } \Gamma_-^A, \\[2mm]
u^A = 0 & \text{on } \Gamma_+^A,
\end{cases}
\tag{10}
$$

In order to write a weak formulation of this problem, we introduce the following function spaces:

$$
\begin{aligned}
V &:= \left\{ v \in H^1(\Omega) : v(L,z) = e^{i\alpha L} v(0,z),\ z \in (0, L_t) \right\}, \\
V^A &:= \left\{ v^A \in H^1(\Omega^A) : v^A(L,z) = e^{i\alpha L} v^A(0,z),\ z \in (-\delta_1, 0) \cup (L_t, L_t + \delta_2), \right. \\
&\qquad\qquad \left. v^A = 0 \text{ on } \Gamma_-^A \cup \Gamma_+^A \right\}.
\end{aligned}
$$

We consider test functions $(v, v^A) \in V \times V^A$ such that $v = v^A$ on $\Gamma_- \cup \Gamma_+$. Multiplying the first equation by v and the second one by v^A, integrating by parts and using the remaining equations, we are lead to the following problem: Find $(u, u^A) \in V \times V^A$ such that $u = u^A + u_{\text{inc}}$ on Γ_-, $u = u^A$ on Γ_+ and

$$
\begin{aligned}
&\int_\Omega \left(B\nabla u \cdot \nabla \overline{v} - k_0^2 b u \overline{v} \right) dx\,dz \\
&+ \int_{\Omega^A} \left(\gamma \frac{\partial u^A}{\partial x}\frac{\partial \overline{v^A}}{\partial x} + \frac{1}{\gamma}\frac{\partial u^A}{\partial z}\frac{\partial \overline{v^A}}{\partial z} - \gamma k_0^2 u^A \overline{v^A} \right) dx\,dz = \int_{\Gamma_-} \frac{\partial u_{\text{inc}}}{\partial z}\overline{v}\,ds
\end{aligned}
\tag{11}
$$

$\forall (v, v^A) \in V \times V^A : v = v^A$ on $\Gamma_- \cup \Gamma_+$.

9

4. Finite element discretization

Let $\{\mathcal{T}_h\}_{h>0}$ be a regular family of triangulations of $\Omega \cup \Omega^A$, where each triangle lies in either Ω or Ω^A, so that the triangles match on the common interfaces Γ_- and Γ_+. As usual, h denotes the mesh-size (diameter of the larger triangle in $\mathcal{T}_h$). Given $k \geq 1$ let

$$
\begin{aligned}
V_h &:= \{v_h \in V : v_h|_T \in \mathbb{P}_k(T) \ \forall T \in \mathcal{T}_h : T \subset \overline{\Omega}\}, \\
V_h^A &:= \{v_h^A \in V^A : v_h^A|_T \in \mathbb{P}_k(T) \ \forall T \in \mathcal{T}_h : T \subset \overline{\Omega^A}\},
\end{aligned}
$$

where $\mathbb{P}_k(T)$ is the set of polynomials of degree not greater than k over the element T.

We introduce the discrete problem associated to Eq. (11): Find $(u_h, u_h^A) \in V_h \times V_h^A$ such that $u_h = u_h^A + I(u_{\text{inc}})$ on Γ_-, $u_h = u_h^A$ on Γ_+ and

$$
\begin{aligned}
&\int_\Omega \left(B\nabla u_h \cdot \nabla \overline{v_h} - k_0^2 b u_h \overline{v_h} \right) dx\,dz \\
&+ \int_{\Omega^A} \left(\gamma \frac{\partial u_h^A}{\partial x} \frac{\partial \overline{v_h^A}}{\partial x} + \frac{1}{\gamma} \frac{\partial u_h^A}{\partial z} \frac{\partial \overline{v_h^A}}{\partial z} - \gamma k_0^2 u_h^A \overline{v_h^A} \right) dx\,dz = \int_{\Gamma_-} \frac{\partial u_{\text{inc}}}{\partial z} \overline{v_h}\,ds
\end{aligned}
\tag{12}
$$

$\forall \, (v_h, v_h^A) \in V_h \times V_h^A : v_h = v_h^A$ on $\Gamma_- \cup \Gamma_+$, where $I(\cdot)$ is the Lagrange interpolation operator in V_h^A.

In order to obtain the matrix form of problem (12), we consider as usual the nodal basis $\{\psi_j\}_{j=1}^{N_h}$ of the finite element spaces V_h and V_h^A. Let us remark that some of the element matrices involve the non integrable function γ. Thus, it is
not clear in principle that the integrals leading to these element matrices must be finite. However, they are finite as we show in what follows.

The integrals that involve unbounded functions are those posed on triangles intersecting either Γ_-^A or Γ_+^A. We focus on the former, but the same analysis holds for the latter. We must distinguish two cases: elements with an edge on Γ_-^A and elements with only one vertex on Γ_-^A. Moreover, according to Eq. (12), we have to consider two type of integrals with unbounded functions:

$$
\int_T \gamma k_0^2 \psi_i \psi_j dx\,dz \quad \text{and} \quad \int_T \gamma \frac{\partial \psi_i}{\partial x} \frac{\partial \psi_j}{\partial x} dx\,dz,
\tag{13}
$$

since the third type $\displaystyle\int_T \frac{1}{\gamma} \frac{\partial \psi_i}{\partial z} \frac{\partial \psi_j}{\partial z}\,dx\,dz$ does not involve unbounded functions.
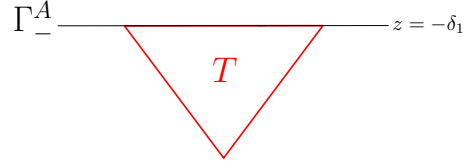
Figure 3: Element T with an edge on Γ^A_-.

First, consider a triangle T with an edge on Γ^A_- as Fig. 3 shows. Since $u^A = 0$ on Γ^A_-, we do not have to consider the basis functions associated to nodes on Γ^A_-. For each of the other basis function ψ_i in T, $\psi_i\big|_{\Gamma^A_-} = 0$ and hence $\frac{\partial \psi_i}{\partial x}\big|_{\Gamma^A_-} = 0$. Then $\frac{\partial \psi_i}{\partial x}$ is a polynomial of degree $k-1$ which vanishes on the line $z = -\delta_1$. Therefore, we may write $\frac{\partial \psi_i}{\partial x}(x,z) = (z+\delta_1)q_i(x,z)$, $q_i \in \mathbb{P}_{k-2}(T)$ and, hence, $\psi_i(x,z) = (z+\delta_1)Q_i(x,z)$, where $Q_i(x,z)$ is a primitive in x of q_i. Then, by using the explicit form (9) of $\gamma(z)$, it follows that

$$\int_T \gamma(z)k_0^2 \psi_i(x,z)\psi_j(x,z)\,dx\,dz = \frac{(1+i)k_0}{\beta}\int_T (z+\delta_1)Q_i(x,z)Q_j(x,z)\,dx\,dz,$$

which involves only polynomial functions. On the other hand, for the second integral in (13), we have

$$\int_T \gamma(z)\frac{\partial \psi_i}{\partial x}(x,z)\frac{\partial \psi_j}{\partial x}(x,z)\,dx\,dz = \frac{1+i}{\beta k_0}\int_T (z+\delta_1)q_i(x,z)q_j(x,z)\,dx\,dz,$$

which also involves only polynomial functions. Therefore, in this case, both integrals in (13) can be safely computed with standard quadrature rules.

Secondly, we consider an element T with only one vertex on Γ^A_-. We will show that for any continuos function $g(x,z)$ the integral $\int_T |\gamma(z)g(x,z)|\,dx\,dz$ is finite, so that both integrals in (13) will be finite.

We use polar coordinates (r,ϕ) centered at the vertex of T on Γ^A_-. We cover the element T by a circular section $\widetilde{T}$ as shown in Fig. 4 with $0 < \phi_1 < \phi_2 < \pi$. Then,

$$
\begin{aligned}
\int_T |\gamma(z)g(x,z)|\,dx\,dz &\leq \int_{\widetilde{T}} \left|\frac{1+i}{\beta k_0(z+\delta_1)}g(x,z)\right|\,dx\,dz \\
&= \sqrt{2}\int_{\phi_1}^{\phi_2}\int_0^R \frac{|g(-r\cos\phi, -\delta_1 + r\sin\phi)|}{\beta k_0 r\sin\phi}r\,dr\,d\phi
\end{aligned}
$$

11

which is finite because $\sin\phi \geq \min\{\sin\phi_1, \sin\phi_2\} > 0$ and g is bounded. Therefore, we conclude that all the integrals that have to be computed in the proposed method are finite in spite of the unbounded character of the function γ.
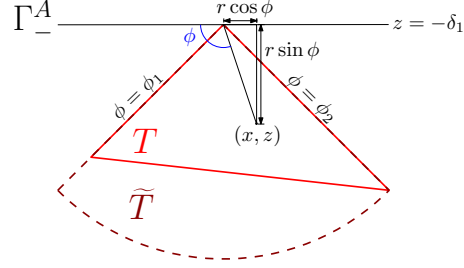

Figure 4: Element T with only one vertex on Γ_-^A. A circular section $\widetilde{T}$ is represented by a polar coordinate system (r, ϕ).

5. Numerical tests

In this section, we report the results obtained by applying the proposed PML technique. We present some numerical examples that allow us to assess the performance of the method. In addition, optimal values of the PML parameters β and $\delta = \delta_1 = \delta_2$ will be experimentally determined. Besides the field u, another quantity of physical relevance is the absorptance defined as follows. Let $\boldsymbol{P} := \dfrac{1}{2\mu_0} Re(\boldsymbol{E} \times \overline{\boldsymbol{H}})$ denote the time-averaged Poynting vector. It represents the time-averaged energy flux density per unit area. The absoprtance is then defined as

$$A := \frac{\displaystyle\int_{\partial\Omega} \boldsymbol{P} \cdot \boldsymbol{\nu}\, ds}{\displaystyle\int_{\Gamma_-} \boldsymbol{P}_{\mathrm{inc}} \cdot \boldsymbol{\nu}\, ds} \tag{14}$$

where $\boldsymbol{P}_{\mathrm{inc}}$ is the time-averaged Poynting vector associated to the incident field. In other words, in an "ideal" solar device, all the energy would be kept inside the structure and thus the absorptance would be equal to one. In order to calculate A, we again decouple the fields in both polarization states. For the s-polarization, we have $\boldsymbol{E} \times \overline{\boldsymbol{H}} = (E_y \overline{H}_z, 0, E_y \overline{H}_x)$. Then, considering the quasi-

12

periodic boundary conditions of E_y, H_x and H_z, by expressing H_x in terms of $u := E_y$ we obtain

$$\int_{\partial\Omega} \boldsymbol{P} \cdot \boldsymbol{\nu} \, ds \quad = \quad \frac{i}{\omega\mu_0^2} Re \left\{ -\int_{\Gamma_-} u \frac{\partial \overline{u}}{\partial z} \, ds + \int_{\Gamma_+} u \frac{\partial \overline{u}}{dz} \, ds \right\}.$$

So, for the s-polarization, the above expression of the absorptance becomes

$$A_s = Re \left\{ \frac{-\int_{\Gamma_-} u \frac{\partial \overline{u}}{\partial z} \, ds + \int_{\Gamma_+} u \frac{\partial \overline{u}}{dz} \, ds}{\int_{\Gamma_-} u_{inc} \frac{\partial \overline{u_{inc}}}{dz} \, ds} \right\}. \tag{15}$$

Proceeding analogously for the p-polarization, the absorptance in this case reads

$$A_p = Re \left\{ \frac{-\int_{\Gamma_-} \frac{1}{\varepsilon_r} \frac{\partial u}{\partial z} \overline{u} \, ds + \int_{\Gamma_+} \frac{1}{\varepsilon_r} \frac{\partial u}{\partial z} \overline{u} \, ds}{\int_{\Gamma_+} \frac{\partial u_{inc}}{\partial z} \overline{u_{inc}} \, ds} \right\}, \tag{16}$$

where the coefficient ε_r on Γ_- or Γ_+ is that of the physical domain.

The domain Ω was discretized into N_e triangles and we have used cubic finite elements ($k = 3$). Let $u_{q,h}$ denote the values of u_q, delivered by our PML finite element method for a specific choice of h, with the polarization state of the incident plane wave being either $q = s$ or $q = p$. The respective approximations of absorptances $A_{q,h}$ are computed from (15) and (16) by using the finite element solution $u_{q,h}$ instead of u_q. Note that the computation of $A_{q,h}$ uses first-order derivatives of the finite element solution. This is the reason why the order of convergence for these quantities will be lower than for the numerical solution $u_{q,h}$, as will be shown below. To avoid this, we have also computed an alternative approximation $\widehat{A}_{q,h}$ of the absorptances by using the approach described in [20], which is based on Fourier expansions of the solution in the unbounded domains $(0, L) \times (-\infty, 0)$ and $(0, L) \times (L_t, \infty)$ and only requires to compute the Fourier coefficients of the finite element solution u_h on Γ_- and Γ_+ (see [20, Section 2] for further details). This approach avoids differentiating the finite element solution and, hence, it should preserve the optimal order of convergence. We point out that this Fourier-based approach is used only to calculate absorptances and not to compute the solution u_h as in the Fourier-FEM method.

13

In all our tests we have taken $L = 400$ nm. The periodic multilayered isotropic dielectric material was taken to comprise $M = 9$ layers of fixed thickness $d = 100$ nm each one. The height of the grating and the thickness of the metal were taken $L_g = 25$ nm and $L_m = 50$ nm respectively. These are representative values for structures suggested in the literature [8, 9, 10]. The relative permittivities ε_r of each material depend on the wavelength λ_0. We have used the physical data from [25] to determine the permittivities for each wavelength. In most of the tests that we report in what follows, we have taken $\lambda_0 = 450$ nm and $\theta = 0$. We will explicitly specify when this is not the case.

5.1. Test 1: Planar backreflector

We have chosen for this test a problem where the solution u_q, $q \in \{s, p\}$ of Eq. (12) can be exactly determined everywhere using a textbook approach [26, Section 1.6]: a metal with a planar metallic backreflector (see Fig. 5).
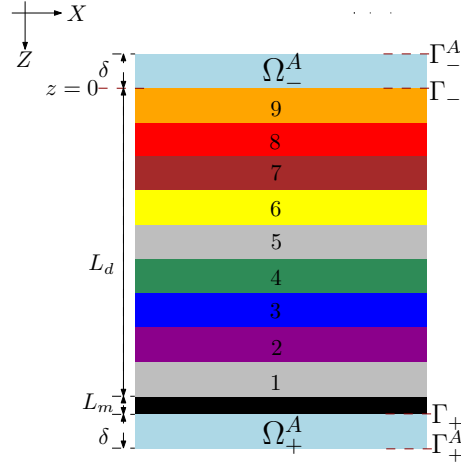
Figure 5: Domain Test 1. The PMLID material of total thickness L_d, comprises $M = 9$ layers on top of a planar metallic backreflector of thickness L_m. The PML regions Ω_+^A and Ω_-^A have a thickness of δ.
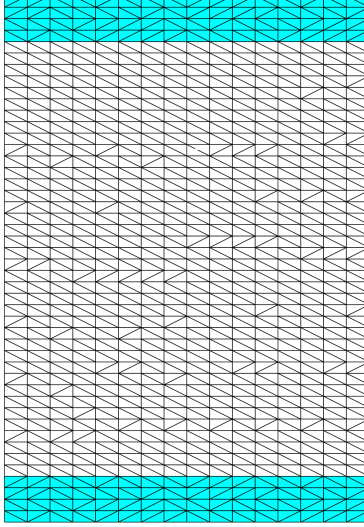
Figure 6: Uniform first mesh discretizing the domain in Fig. 5.

To numerically solve this problem, we have used succesive uniform refinements of the mesh shown in Fig. 6. As it can be seen from this figure, we have not used more refined meshes for the PML than for the rest of the domain.

For each polarization state, we have computed the errors

$$e_{u_q} := \left(\int_\Omega |u_q - u_{q,h}|^2 \right)^{1/2} \quad \text{and} \quad e_{A_q} := |A_q - A_{q,h}|, \quad q \in \{s, p\}. \quad (17)$$

In order to determine the optimal values of the PML thickness δ and the parameter β in the absorbing coefficient (9), we solved the problem with different values of these parameters ($0.1 \leq \beta \leq 5$ and 50 nm $\leq \delta \leq$ 350 nm) and different values of the mesh size h and computed the corresponding errors. First, in results not shown here, we observed that in all cases the optimal value of β is around 0.3. Secondly, also in results not shown, we observed that there is almost no advantage in using $\delta >$100 nm. In fact, the errors with $\delta = 100$ nm and $\delta = 350$ nm differ in less than 1% for all the meshes. Consequently, we chose $\delta = 100$ nm. Let us remark that the thickness of the PML remains constant for different mesh sizes h. One could be tempted to use a PML with a fixed number

15

of element layers, so that its thickness becomes smaller as h goes to zero. We assessed this approach but the results showed that this is not a good strategy because in such case the PML error does not reduce with h.

With this value of δ fixed, we refined the search of an optimal value of the parameter β by solving again the problem with different mesh sizes h. In Fig. 7 we display the error e_{u_q}, $q \in \{s, p\}$ for $\delta = 100$ nm and β varying between 0 and 5, for four succesively refined meshes. The error curves in this figure show that, for β varying between 0.2 and 0.4, the results do not significantly change. In fact, we have repeated the experiments that follow in this section with different values of β in this range and different values of $\delta \geq 100$ nm and the results were essentially the same. Finally, in order to confirm that the optimal value of β is also independent of the wavelength λ_0, we repeated the experiment with different values of this parameter ($\lambda_0 = 600$ nm, $\lambda_0 = 750$ nm and $\lambda_0 = 900$ nm) and in all tests the optimal value of β did not change.

(a)   (b)
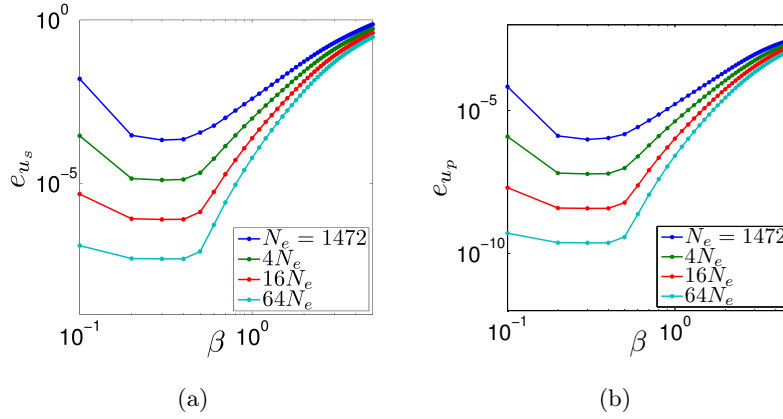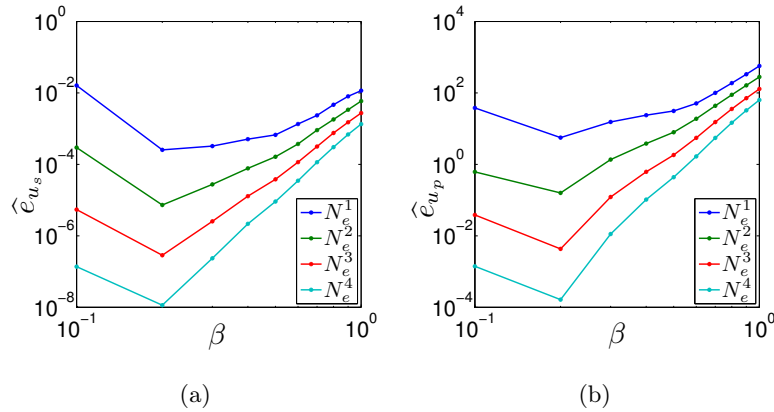
Figure 7: Test 1. Errors e_{u_s} (a) and e_{u_p} (b), for $0 < \beta < 5$, $\delta = 100$ nm, $\lambda_0 = 450$ nm and four succesively refined meshes. N_e: number of elements of the mesh from Fig. 6.

We report in Fig. 8 error curves for e_u and e_A versus the mesh size h for both polarization states. For this test we have used the values $\delta = 100$ nm

16

and $\beta = 0.2$ determined above. These plots show that the error e_u in both polarizations decreases for our PML model with the order $\mathcal{O}(h^4)$ that the theory predicts for the cubic finite elements that have been used. The convergence rate

235 for the absorptance error e_A for both polarizations is only $\mathcal{O}(h^3)$ due to the approximation of the derivatives, as explained above (see (15) and (16)). We have also computed the absorptances $\widehat{A}_{q,h}$ with the above mentioned Fourier-based approach. It can be seen from Fig. 8 that the order of convergence of the errors $e_{\widehat{A}_q} := |A_q - \widehat{A}_{q,h}|$ are again $\mathcal{O}(h^4)$ for the s-polarization and close to

240 $O(h^4)$ for the p-polarization.
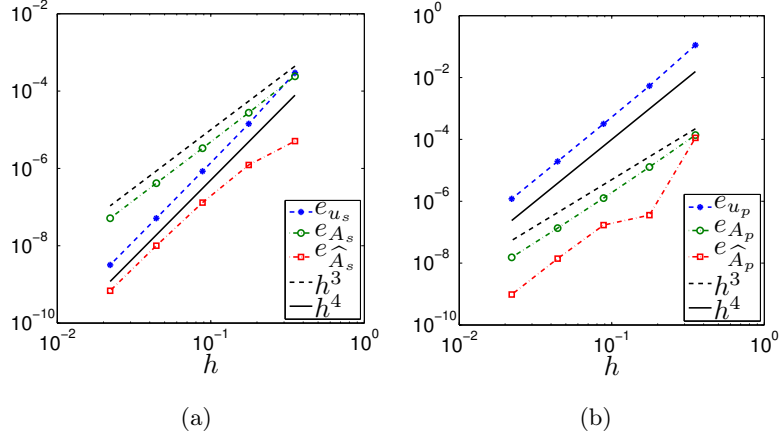
Figure 8: Test 1. Computed errors e_u, e_A and $e_{\widehat{A}}$ versus the mesh size h: (a) s-polarization and (b) p-polarization.

5.2. Test 2: Periodic backreflector with rectangular corrugations

In the following section, we report the same results as in the previous test for a corrugated surface relief, instead of a planar metallic blackreflec-

245 tor. Since an exact solution u cannot be found for the chosen backreflector, we denote by $u_{q,h}^{FEM}$ a FEM solution obtained with the method proposed in [20]. Let us remark that the two methods differ only in the way the radiation conditions at infinity are modeled. While in our case this is done

17

by means of a PML technique, the method in [20] uses a Fourier series ap-

250   proach, which makes the latter significantly more expensive. We compute
the quantities $\widehat{e}_{u_q} := \left(\int_\Omega |u_{q,h}^{FEM} - u_{q,h}|^2 \right)^{1/2}$, $\widehat{e}_{A_q} := |A_{q,h}^{FEM} - A_{q,h}|$ and
$\widehat{e}_{\widehat{A}_q} := |A_{q,h}^{FEM} - \widehat{A}_{q,h}|$.

Let us emphasize that $\widehat{e}_{u_q}$, $\widehat{e}_{A_q}$ and $\widehat{e}_{\widehat{A}_q}$ are not actual errors but measures
of the differences between the values obtained with the proposed PML approach

255   and the more expensive Fourier-FEM approach proposed in [20]. In spite of this
fact, in what follows we will make an abuse of language and call these quantities
'errors'.

Analogously to Test 1, first we determined the optimal parameters β and
δ. The experiments with different δ lead to the same conclusion as in the

260   previous test. No significant difference was observed between the results with
$\delta = 100$ nm and larger δ. Consequently, we have chosen again $\delta = 100$ nm and
we have computed the error $\widehat{e}_{u_q}$, $q \in \{s, p\}$ for different values of β. We have
limited the search to β varying between 0 and 1.

Figure 9: Test 2. Errors $\widehat{e}_{u_s}$ (a) and $\widehat{e}_{u_p}$ (b), for $0 < \beta < 1$, $\delta = 100$ nm,
$\lambda_0 = 450$ nm and four successively refined meshes, where the number of elements
of the meshs are: $N_e^1 = 1504$, $N_e^2 = 5888$, $N_e^3 = 23552$ and $N_e^4 = 92208$.

265   Fig. 9 shows the errors $\widehat{e}_{u_q}$, $q \in \{s, p\}$, for four successively refined meshes.

In this case, the curves show that $\beta = 0.2$ is the optimal parameter for both polarizations. Finally we have computed the errors $\widehat{e}_{u_q}$ and $\widehat{e}_{A_q}$, $q \in \{s, p\}$. In Table 1 we display the values obtained with $\beta = 0.2$ and $\delta = 100$ nm and different values of h. The corresponding curves are shown in Fig. 10.

Table 1: Test 2. Errors $\widehat{e}_{u_q}$ and absorptance errors $\widehat{e}_{A_q}$ for both polarizations ($q = s$ and $q = p$) and succesively refined meshes.

N_e	h	$\widehat{e}_{u_s}$	$\widehat{e}_{u_p}$	$\widehat{e}_{A_s}$	$\widehat{e}_{A_p}$
1504	35.36	1.7235e-04	1.2489e-02	8.4658e-05	1.9036e-03
5888	17.68	5.4400e-06	4.0230e-04	8.5001e-06	1.4661e-04
23552	8.84	2.3305e-07	1.0651e-05	9.8752e-07	2.6806e-05
92208	4.42	9.7951e-09	4.0624e-07	1.2448e-07	3.9086e-06

(a)   (b)
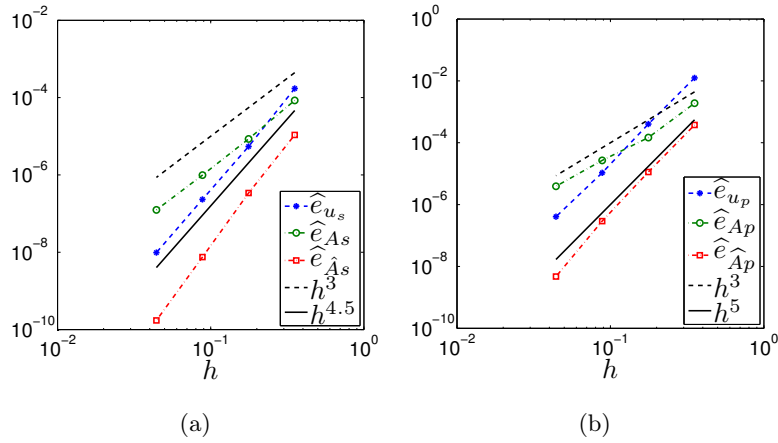
Figure 10: Test 2. Computed errors $\widehat{e}_u$, $\widehat{e}_A$ and $\widehat{e}_{\widehat{A}}$ versus the mesh size h: (a) s-polarization and (b) p-polarization.

The reported results show that the rate of convergence of errors $\widehat{e}_{u_q}$ are higher than expected. Indeed, these terms are $\mathcal{O}(h^{4.5})$ ($q = s$) and $\mathcal{O}(h^5)$ ($q = p$) while the order of convergence of the finite element method is expected to be at most $\mathcal{O}(h^4)$. As a consequence, the use of the proposed PML approach will lead

19

essentially to the same results as the method from [20], but with a less expensive computational cost. In addition, as in the previous test, the absorptance errors $\widehat{e}_{A_q}$ were $\mathcal{O}(h^3)$ instead of $\mathcal{O}(h^4)$. However, for realistic meshes, these errors are negligible compared to the errors of the finite element method. This fact justifies the use of the proposed PML approach in order to save computer cost.

6. Conclusions

We have introduced a novel PML technique for finite element calculations of diffraction by metallic surface-relief gratings and tested it by simulating a structure comprising an isotropic dielectric multilayer material and a metallic backreflector. We have numerically shown that the results are robust with respect to the thickness δ of the PML, the absorbing parameter β and the wavelength λ_0. Moreover, since the proposed PML is based on a non-integrable absorbing function, small values of δ can be considered which would considerably reduce the computational cost compared to the Fourier-FEM approach. In addition, we show that the entries of the finite element matrix are finite even though they involve a non-integrable function.

Acknowledgments

References

[1] L. M. Anderson, Parallel-processing with surface plasmons: a new strategy for converting the broad solar spectrum, in: Proc. 16th IEEE Photovoltaic Specialist Conf., Vol. 1, San Diego, CA, 1982, pp. 371–377.

[2] L. M. Anderson, Harnessing surface plasmons for solar energy conversion, Proc. SPIE 408 (1983) 172–178.

[3] P. Sheng, A. N. Bloch, R. S. Stepleman, Wavelength-selective absorption enhancement in thin-film solar cells, Appl. Phys. Lett. 43 (1983) 579–581.

[4] C. Heine, R. H. Morf, Submicrometer gratings for solar energy applications, Appl. Opt. 34 (1995) 2476–2482.

[5] S. Mokkapati, K. R. Catchpole, Nanophotonic light trapping in solar cells, J. Appl. Phys. 112 (2012) 101101.

[6] M. Faryad, A. Lakhtakia, Enhancement of light absorption efficiency of amorphous-silicon thin-film tandem solar cell due to multiple surface-plasmon-polariton waves in the near-infrared spectral regime, Opt. Eng. 52 (8) (2013) 087106.

[7] M. Wellenzohn, R. Hainberger, Insights in the light trapping effect in silicon solar cells with backside diffraction gratings, J. Photon. Energy 3 (1) (2013) 034595–034595.

[8] M. Faryad, A. S. Hall, G. D. Barber, T. E. Mallouk, A. Lakhtakia, Excitation of multiple surface-plasmon-polariton waves guided by the periodically corrugated interface of a metal and a periodic multilayered isotropic dielectric material, J. Opt. Soc. Am. B. 29 (2012) 704–713.

[9] M. Faryad, A. Lakhtakia, Grating-coupled excitation of multiple surface plasmon-polariton waves, Phys. Rev. A. 84 (2011) 033852.

[10] M. Faryad, A. Lakhtakia, On surface plasmon-polariton waves guided by the interface of a metal and a rugate filter with sinusoidal refractive-index profile, J. Opt. Soc. Am. B. 27 (2010) 2218–2223.

[11] M. E. Solano, M. Faryad, P. B. Monk, T. E. Mallouk, A. Lakhtakia, Periodically multilayered planar optical concentrator for photovoltaic solar cells, Appl. Phys. Lett. 103 (2013) 191115.

21

[12] M. E. Solano, G. D. Barber, A. Lakhtakia, M. Faryad, P. B. Monk, T. E. Mallouk, Buffer layer between a planar optical concentrator and a solar cell, AIP Advances 5.

[13] B. Gralak, Exact modal methods, in: E. Popov (Ed.), Gratings: Theory and Numeric Applications, Institut Fresnel, CNRS, Universié d'Aix-Marseille, 2012, pp. 373–427.
URL http://http://www.fresnel.fr/files/gratings/Chapter10.pdf

[14] V. Jandhyala, D. Sengupta, B. Shanker, E. Michielssen, M. Feng, G. Stillman, Efficient electromagnetic analysis of two-dimensional finite quasi-random gratings for quantum well infrared photodetectors, J. Appl. Phys. 83 (1998) 3360–3363.

[15] G. Granet, L. B. Andriamanampisoa, K. Raniriharinosy, A. M. Armeanu, K. Edee, Modal analysis of lamellar gratings using the moment method with subsectional basis and adaptive spatial resolution, J. Opt. Soc. Am. A. 27 (2010) 1303–1310.

[16] N. Chateau, J.-P. Hugonin, Algorithm for the rigorous coupled-wave analysis of grating diffraction, J. Opt. Soc. Am. A. 11 (1994) 1321–1331.

[17] P. Lalanne, G. M. Morris, Highly improved convergence of the coupled-wave method for tm polarization, J. Opt. Soc. Am. A. 13 (1996) 779–784.

[18] P. B. Monk, Finite Element Methods for Maxwell's Equations, Oxford University Press, 2012.

[19] H. Ichikawa, Electromagnetic analysis of diffraction gratings by the finite-difference time-domain method, J. Opt. Soc. Am. A. 15 (1998) 152–157.

[20] M. E. Solano, M. Faryad, A. Lakhtakia, P. B. Monk, Comparison of rigorous coupled-wave approach and finite element method for photovoltaic devices with periodically corrugated metallic backreflector, J. Opt. Soc. Am. A 31 (2014) 2275–2284.

[21] Z. Chen, W. Haijun, An adaptive finite element method with perfectly matched absorbing layers for the wave scattering by periodic structures, SIAM J. Numer. Anal. 41 (3) (2004) 799–826.

[22] A. Bermúdez, L. Hervella-Nieto, A. Prieto, R. Rodríguez, An optimal perfectly matched layer with unbounded absorbing function for time-harmonic acoustic scattering problems, J. Comp. Phys. 223 (2) (2007) 469–488.

[23] A. Bermúdez, L. Hervella-Nieto, A. Prieto, R. Rodríguez, Perfectly matched layers for time-harmonic second order elliptic problems, Arch. Computat. Methods Eng. 17 (2010) 77–107.

[24] A. Bermúdez, L. Hervella-Nieto, A. Prieto, R. Rodríguez, An exact bounded perfectly matched layer for time-harmonic scattering, SIAM J. Sci. Comput. 30 (2007) 312–338.

[25] A. S. Hall, M. Faryad, G. D. Barber, L. Liu, S. Erten, T. S. Mayer, A. Lakhtakia, T. E. Mallouk, Broadband light absorption with multiple surface plasmon polariton waves excited at the interface of a metallic grating and photonic crystal, ACS Nano 7 (2013) 4995–5007.

[26] M. Born, E. Wolf, Principles of Optics, 6th ed. Cambridge University, 1980.

Centro de Investigación en Ingeniería Matemática (CI²MA)

PRE-PUBLICACIONES 2016 - 2017

CENTRO DE INVESTIGACIÓN EN
INGENIERÍA MATEMÁTICA (CI²MA)
Universidad de Concepción

Casilla 160-C, Concepción, Chile
Tel.: 56-41-2661324/2661554/2661316
http://www.ci2ma.udec.cl